ELSEVIER

Journal of Nuclear Materials 318 (2003) 102–108

journal of nuclear materials

www.elsevier.com/locate/jnucmat

SNS target tests at the LANSCE-WNR in 2001 – Part II

J.D. Hunn *, B.W. Riemer, C.C. Tsai

Oak Ridge National Laboratory, P.O. Box 2008, Building 4500S, MS-6138, Oak Ridge, TN 37831-6138, USA

Abstract

It has been observed that stopping of an 800 MeV proton pulse in liquid mercury, such as in the United States Spallation Neutron Source (SNS), leads to cavitation that can affect the mercury vessel. This paper discusses pitting that was observed on mercury container walls after 100–200 proton pulses obtained at the Los Alamos Neutron Science Center Weapons Neutron Research facility (LANSCE-WNR). It was found that the degree of cavitation-induced pitting was dependent on the geometry and composition of the container. As expected, very hard surfaces were particularly effective for resisting deformation from cavity collapse.

PACS: 47.55.Bx

1. Introduction

In Part I [1], we discussed the experimental motivation and specific target conditions for a series of tests to look at the effect of United States Spallation Neutron Source (SNS)-relevant proton beam pulses on the inner surfaces of mercury-filled containers. Deformation pits have been observed on these surfaces and linked to cavitation of the mercury induced by pressure pulses caused by the local thermal expansion of the mercury along the proton beam path. Cavitation in a liquid medium occurs when local tensile forces are sufficient to cause holes, filled with entrained gas or vapor, to form in the medium. When those cavities encounter sufficiently higher pressure they will collapse. If that collapse occurs near a solid surface, the in-rush of liquid and associated shock wave can cause deformation in the surface [2].

2. Procedure

From the split Hopkinson pressure bar (SHPB) experiments discussed in Part I, it was predicted that deformation pits would be on the order of 10 μm. To permit the observation of micron-size surface features, specimen surfaces were prepared by machining flat and polishing. Polishing involved grinding with silicon carbide paper in steps of decreasing grit size (from 240 grit down to 4000 grit). This was followed by vibratory polishing in diamond suspensions of 15, 6, and 3 μm.

Some of the specimens were annealed after polishing. For 316LN, we used a standard austenitizing anneal at 1050 °C for 30 min in vacuum. On some of the thinner specimens, intermediate annealing and careful machining were also necessary in order to keep the surfaces flat.

Even with the metalographic polish, there were still some defects scattered about the surface that could be misconstrued as cavitation damage after the irradiation. For this reason, specimen surface topography was carefully mapped by SEM prior to irradiation. SEM was carried out using an ISI Cl-8 microscope capable of handling specimens up to 20 cm diameter and a Philips XL-30 FEG microscope with a computer-controlled stage and capable of higher resolution but limited to 10 cm diameter plates. A reproducible pre-irradiation inspection strategy was conceived which would yield an acceptable balance between areal coverage, feature resolution, and inspection effort. In the July 2001 tests, the center of the specimen was marked with an X and 25 overlapping images were obtained with the ISI CL-8, moving out in each of four directions (0°, 90°, 180°, and 270°). A resolution of 1.7 μm/pixel and a digital capture

* Corresponding author. Tel.: +1-865 574 2480; fax: +1-865 241 3650.

E-mail address: hunnjd@ornl.gov (J.D. Hunn).

0022-3115/03/$ - see front matter © 2003 Elsevier Science B.V. All rights reserved.
doi:10.1016/S0022-3115(03)00074-6

size of 600×541 pixels resulted in a mapped area of two perpendicular strips 50 mm $\times$ 1 mm, centered on the flange. In the December 2001 tests, the specimens were indented with a 5×5 array using a microhardness tester. The indents of the array were spaced 5 mm apart in two orthogonal directions to form a 20 mm square. The areas surrounding each of these indents were imaged with the SEM at two magnifications. On the ISI CL-8 the resolutions were 2.3 and 0.46 μm/pixel with a digital capture size of 500×500 pixels. On the Philips XL-30 the resolutions were 0.75 and 0.19 μm/pixel with a capture size of 1273×968 pixels.

After irradiation, specimens were cleaned to remove smearable radioactive contamination as outlined in Part I and the surface mapping procedures were repeated. This allowed for the direct comparison of the same surface areas before and after irradiation. Higher resolution images were obtained of select features which had appeared during the test. The thin windows of the four specimens in the July 2001 test were also cut out and examined in the Philips XL-30. Further details of the irradiations are given in Part I.

3. Results

In Part I, we described the target specifications and irradiation conditions and described the differences in the individual specimen flanges. In this section we discuss the effects of the mercury cavitation on the specimen surfaces.

Evidence for the initiation of cavitation-induced erosion was found in the form of pits in the polished surfaces. These pits showed two distinct features, dishes and craters. Dishes were formed by inelastic deformation of the flat, polished surface. Fig. 1 shows a typical dish. Shadowing of the electrons collected by the secondary electron detector which sits at about a 45° angle to the surface produces the light/dark shading that makes the pit topography visible. The parallel striations within each crystal grain are 'slip lines' formed by adjacent planes of atoms sliding over one another. This is evidence that mechanical deformation has occurred. Where the pits did not overlap, the dishes were typically round and symmetric, suggesting that they were formed by the collapse of a single bubble. The dark spots are relatively deep, sharp-walled craters out of which few, if any, secondary electrons reach the detector. Craters were formed by the forceful removal of material from the surface. These craters were found near the bottom of many of the dishes, especially the larger ones (Fig. 2). The shapes of the craters were very irregular and the side walls had a high aspect ratio. Fig. 3 shows a close-up image of a crater.

The two targets tested in July 2001, LE3 and LE4, were essentially identical, as described in Part I. Fig. 4 shows an area near the center of the front flange of LE3, a 1.5-mm-thick annealed 316LN stainless steel window.

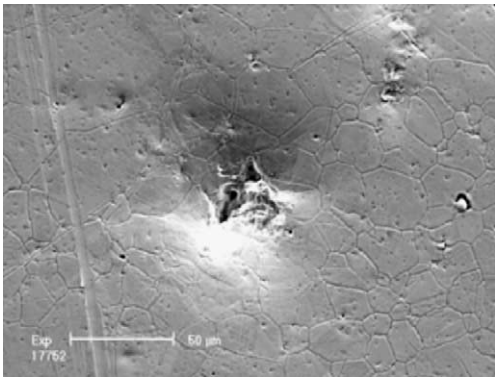

Fig. 2. Typical crater at the bottom of a pit. Material: annealed stainless steel.

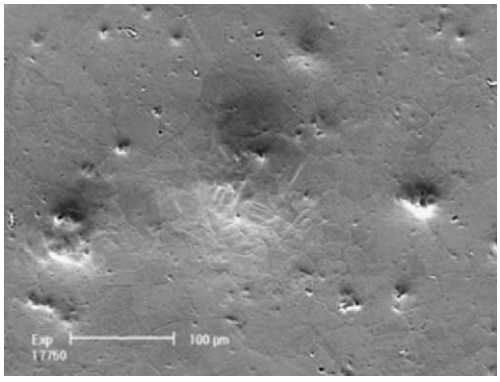

Fig. 1. Central pit shows typical dished depression. Deformation slip lines are evident. Material: annealed stainless steel.

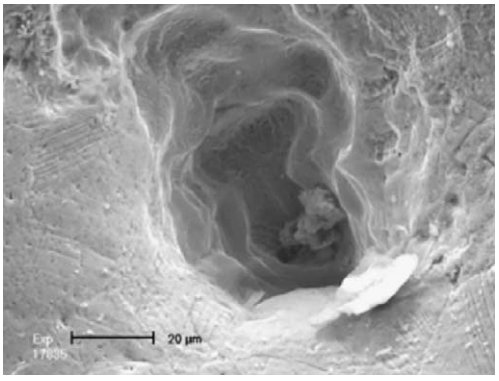

Fig. 3. Close-up of a typical crater exhibiting steep sidewalls. Material: annealed stainless steel.

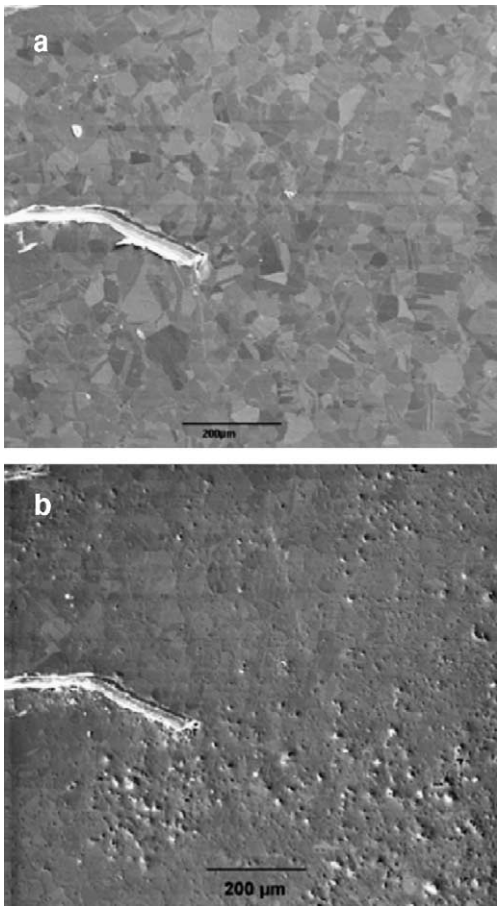

Fig. 4. Just off center of LE3 front flange (a) before and (b) after 200 pulses. Material: annealed stainless steel.

Comparison of the pre- and post-irradiation images clearly shows evidence for surface pitting during the test. The 5–20 μm pits in the upper half of Fig. 4(b) were typical of what were seen scattered over the entire surface. In the lower half of the figure can be seen a higher density cluster of slightly larger pits. This clustering was observed in several regions on the flange. One big cluster of especially large pits, up to 200 μm diameter, could be seen even with the unaided eye. Part of this cluster is shown in Fig. 5. Laser profilometry showed some of these pits to be up to 70 μm deep. Figs. 1 and 2 show some of these pits at higher magnification. This one area of heavy damage on the specimen, visible with the unaided eye, was a common observation in our tests. As discussed in Part I, we believe this heavy damage is a focusing effect related to the cylindrical shape of the target volume. This hypothesis is being tested in some ongoing experiments.

The rear flange of LE3 and the front flange of LE4, both annealed 316LN, showed similar results to those of

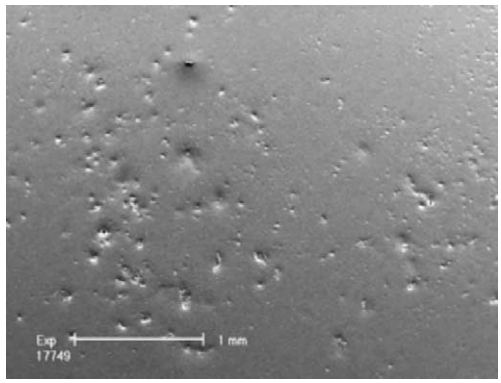

Fig. 5. LE3 front flange after 200 pulses, heavily damaged region. Material: annealed stainless steel.

the LE3 front flange. The rear window of LE4 was surface hardened by the Kolsterization [1] process described in Part I. Small pits were not as obvious on the Kolsterized surface because there were more than a factor of 10 fewer of them (none in clusters), and partly due to the fact that the Kolsterizing treatment roughened the polished surface making inspection more difficult. In addition to a few isolated small pits, a cluster of larger pits was also seen on this specimen. Fig. 6 shows the heavily damaged area from the two rear flanges. Again, the flange from LE4 was not as heavily damaged as its counterpart due to the Kolsterizing surface treatment that increased the surface hardness by about a factor of 8. Qualitatively, the pits were the same on the Kolsterized flange, but they appeared smaller and at a lower density.

The front flange of LE5, a 10-mm-thick Kolsterized 50% cold-worked 316LN plate, showed little to no pitting in the SEM inspection, which was capable of identifying pit features larger than 1 μm. Fig. 7 shows the Kolsterized surface before and after irradiation. The high density of deformation slip lines in the pre-inspection image was typical of the Kolsterizing process which injects a high concentration of carbon into the surface. In the post-irradiation image, it was evident that a surface film had blistered and partially exfoliated. The surface in the exfoliated area was still as hard as the original Kolsterized surface and there was still no evidence of pitting in these areas. Laser profiling showed that the exfoliated film was 3–5 μm thick, about 10% of the Kolsterized layer. X-ray diffraction analysis showed the presence of an iron carbide phase on the surface of the Kolsterized layer which may be what was flaking off.

[1] Kolsterizing is a registered trademark of the Bodycote Company. Bodycote Hardiff bv, Paramariboweg 45, NL-7333 PA Apeldoorn, The Netherlands.

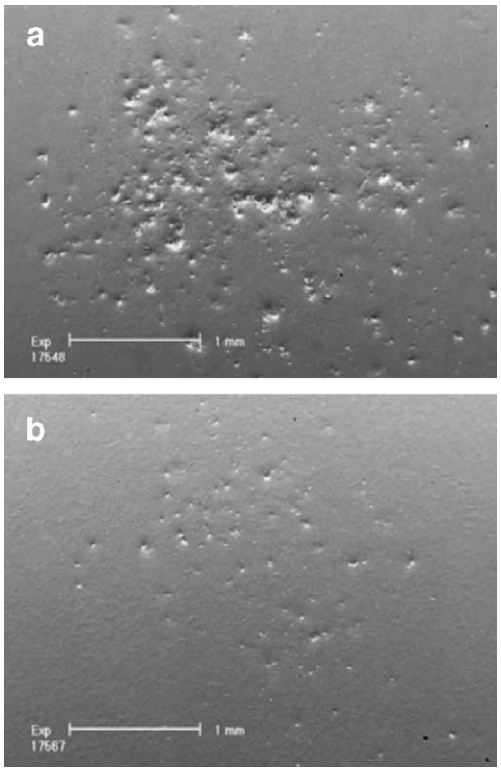

Fig. 6. (a) LE3 rear flange and (b) LE4 rear Kolsterized flange, heavily damaged region.

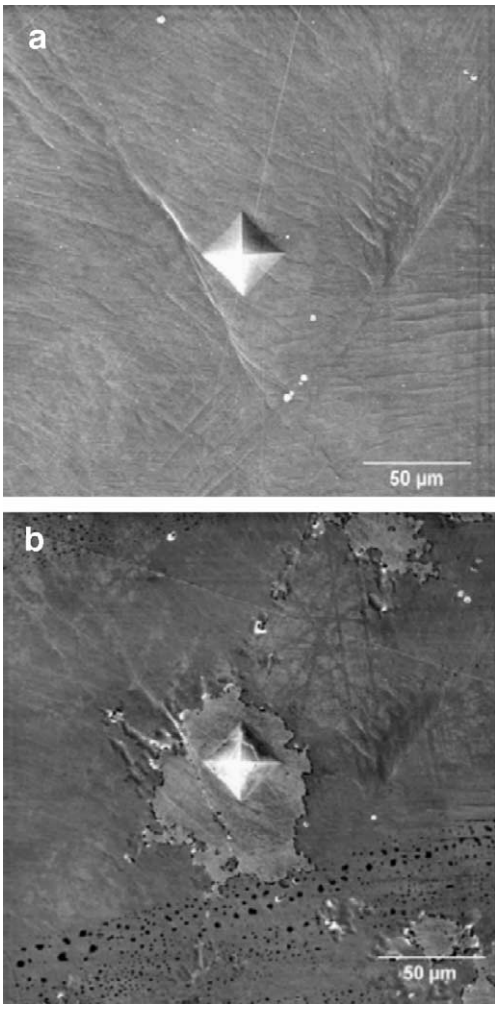

Fig. 7. Front flange of LE5 (a) before and (b) after irradiation.

The rear flange of LE5, 10-mm-thick annealed 316LN, had an area of damage that was visible with the unaided eye. This area was centered on the flange and was approximately 40 mm diameter. These visible spots of damage were actually 100–200 μm diameter clusters of smaller pits. One such cluster is shown in the center of Fig. 8. This differed significantly from what was observed in LE3 and LE4, and in general on all the 1–2-mm-thick windows. There the visual damage consisted of larger, isolated, 100–200 μm diameter pits in a 1–5 mm diameter cluster. Presumably, the change was due to the difference in window thickness, which would change the acoustics, the local strain, and the amount of motion in the window. In addition to the visible clusters on the rear flange of LE5, there were also isolated pits up to 50 μm diameter scattered over the entire specimen surface (Fig. 8).

The rear flange of LE6, 10-mm-thick Nitronic-60, showed no improvement over the annealed 316LN in LE5. Again 100–200 μm diameter clusters could be seen with the unaided eye, covering an area of approximately 40 mm diameter. The remainder of the flange was randomly freckled with pits up to 50 μm diameter.

The front flange of LE6 was made of 10-mm-thick Stellite-6B, the second hardest surface in the test after the Kolsterized steel. This material's response was distinctly different from the others tested. A 3 mm diameter cluster of pits in the area where the proton beam had passed through could be seen with the unaided eye. This was different from the position of the large pit clusters observed on the thin windows, as discussed in Part I. The pit cluster was also characteristically different in that it consisted almost entirely of large pits, 150–200 μm diameter (Fig. 9), as opposed to the continuous size distribution observed on other specimens. The unusual size distribution in the pit cluster suggests that the Stellite material was able to resist all but the most violent impacts. There was also no indication of the small generalized pitting that was observed on the other flanges (with the exception of the Kolsterized surface).

The front flange of LE7, 6-mm-thick annealed 316LN, was mounted on a conical offset, as discussed in Part I. The conical adapter was 3.2 cm deep, and

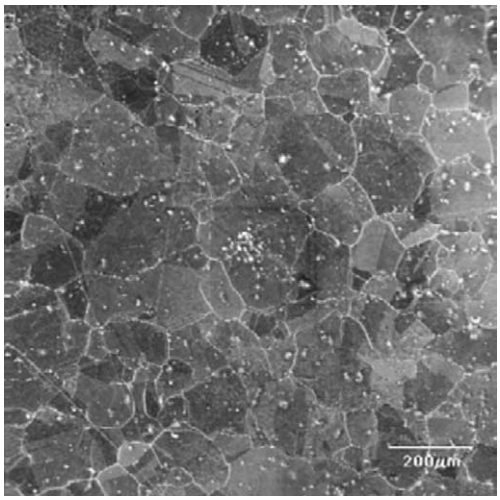

Fig. 8. Rear flange of LE5 after 200 pulses. Material: annealed stainless steel.

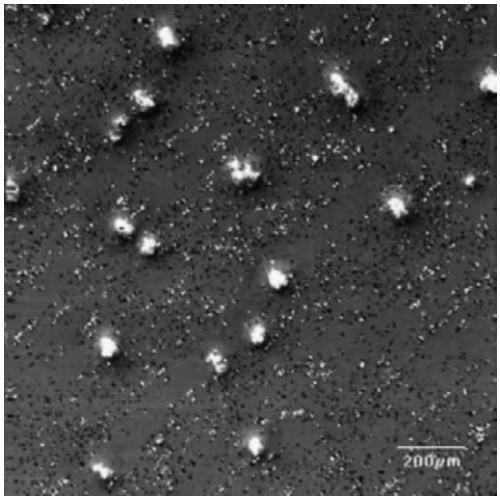

Fig. 9. Front flange of LE5 after 200 pulses. Material: Stellite-6B. The small black and white specks are pre-existing features (carbides and polishing defects).

reduced the window diameter from 10 to 3.8 cm. There was a 2 mm diameter cluster of pits up to 100 μm diameter in the center of the specimen which could be seen with the unaided eye. In addition to this damage, there were smaller, randomly distributed pits over the entire surface. Fig. 10 shows these small pits as well as a few of the larger pits in the center cluster. The size and density of the general pitting dropped off sharply as a function of distance from the center, suggesting that the conical section may have acted to concentrate the pressure pulse toward the center of the front flange.

The rear flange of LE7, 1.5-mm-thick annealed 316LN, showed the cluster of large pits and general

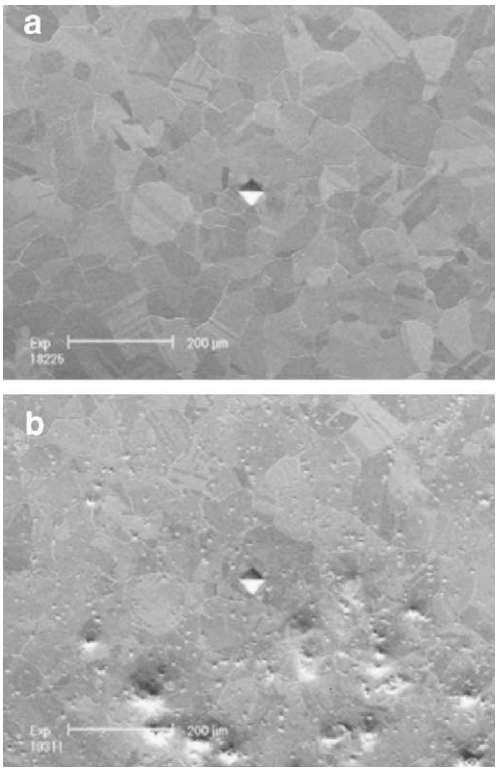

Fig. 10. Front flange of LE7 with conical offset (a) before and (b) after 100 pulses. Material: annealed stainless steel.

distribution of small pits observed in other thin window LE-type targets such as LE-3 and LE-4. A liquid lead bismuth target, which also used the LE geometry and thin annealed 316LN windows, also showed similar damage.

One rectangular bodied target was irradiated in the December test in order to investigate the effect of the non-prototypical cylindrical target shape on the observed pitting. All specimen plates were Nitronic-60 and there was a 6-mm-thick plate inset 3 mm from the front to represent the double-wall SNS target vessel design. The geometry of this target is shown in Fig. 14 of Part I, with the specimen surfaces labeled 1–4. The first two surfaces, bounding the 3-mm-thin mercury layer, showed more visible damage than any other test. Both of these surfaces had a 20–25 mm diameter cluster of pits up to 100 μm diameter. This heavily damaged region corresponded to the area through which the proton beam passed. Surfaces 3 and 4, which bounded the bulk mercury region, did not show any damage visible with the unaided eye. However, they were not completely free of damage. There were a few small 5–10 μm pits in one region on surface 4. On surface 3, there were a few small 1–2 μm pits scattered over the entire plate. In addition, there was an area of heavier pitting where pit sizes

ranged up to 20 μm diameter. This area corresponded to the same area of heavy pitting on the opposite side (surface 2). Because of the complication of the double-wall structure, it is not clear whether the absence of large pits on the windows of the bulk region fully supports the hypothesis of pressure wave focusing in the cylindrical target bodies. More tests are being performed.

The characteristics of the pits on the insert (surfaces 2 and 3) was different from that observed on other specimens. Fig. 11 shows a pit in surface 2. In addition to the dished depression and the sharp-walled crater, there is an intermediate area where material has been removed or smeared at an oblique angle. These scooped out areas tended to show a spiral character as can be seen in Fig. 12.

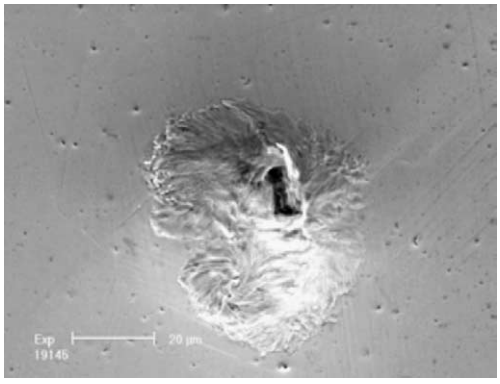

Fig. 11. Pit in surface 2 of the rectangular target after 200 pulses. Material: 20% cold-worked Nitronic-60.

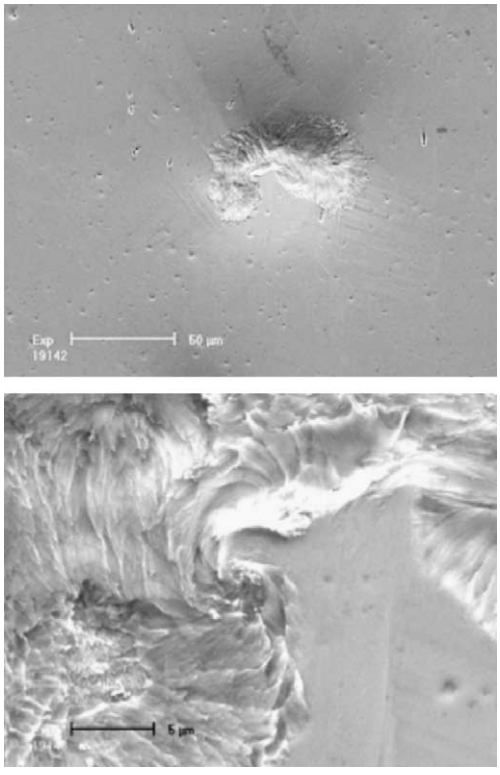

Fig. 12. Pit (at two magnifications) in surface 2 of rectangular target after 200 pulses. Material: 20% cold-worked Nitronic-60.

4. Conclusions

It has been shown that when a mercury-filled stainless steel container is subjected to SNS-relevant proton beam pulses, the walls of that container sustain damage in the form of pits. The pits are permanent depressions in the surface, sometimes accompanied by craters where material has been removed. These pits have the same characteristics as cavitation-induced damage in other liquids and it is reasonable to assume that they are formed by collapse of cavities in the mercury near the surface.

We have observed two types of pitting. Small pits, distributed on the surface in a somewhat random fashion were observed on most of the specimens. In addition to this damage, large pits measuring up to 200 μm in diameter were usually observed clustered in one location on the window. These clusters of large pits were visible with the unaided eye. It is conjectured that this heavier damage may be an artifact of the target container geometry resulting in a focusing of the pressure waves. The first test of this theory using a non-cylindrical geometry was inconclusive but promising. More tests are currently in progress. The heavy damage is also apparently influenced by the thickness of the window. Excluding the two unusual geometries, windows thinner than 2 mm showed large pit clusters that were different in characteristic and relative location to the proton beam than 8–10-mm-thick windows. Thicker windows would exhibit less strain and reflect the pressure pulses differently, but it is not understood how this explains the observed differences.

Increasing the surface hardness with a treatment such as Kolsterizing clearly had a mitigating effect on the observed pitting. Apparently the combination of thick-wall, cold-worked 316LN, and Kolsterizing was sufficient to prevent or at least delay the incubation of cavitation erosion. A Kolsterized surface on a thin-wall annealed 316LN specimen showed pitting but at about 1/10 the level of a similar specimen without the Kolsterizing treatment. The critical difference between these two may be the hardness of the underlying material. Stellite, which was the second hardest material appeared to be resistant to formation of small pits but still

succumbed to the heavier impacts which were responsible for creating the observed clusters of large pits. In that material only 150–200 μm pits were observed.

Acknowledgements

As mentioned in Part I, many people were involved in designing these tests and assembling and irradiating the targets. We would also like to thank D.B. Smith and M.J. Gardner for SEM support. Thanks also to K. Farrell for helpful discussions of our results. SNS is managed by UT-Battelle, LLC, under contract DE-AC05-00OR22725 for the US Department of Energy.

References

[1] B.W. Riemer, J.R. Haines, J.D. Hunn, D.C. Lousteau, T.J. McManamy, C.C. Tsai, these Proceedings. doi:10.1016/S0022-3115(03)00076-X.
[2] A. Philipp, W. Lauterborn, J. Fluid Mech. 361 (1998) 75.